J Geod (2009) 83:773–785
DOI 10.1007/s00190-008-0296-8

ORIGINAL ARTICLE

Accuracy assessment of the GPS-based slant total electron content

Claudio Brunini · Francisco Javier Azpilicueta

Received: 22 April 2008 / Accepted: 15 December 2008 / Published online: 6 January 2009

Abstract The main scope of this research is to assess the ultimate accuracy that can be achieved for the slant total electron content (sTEC) estimated from dual-frequency global positioning system (GPS) observations which depends, primarily, on the calibration of the inter-frequency biases (IFB). Two different calibration approaches are analyzed: the so-called satellite-by-satellite one, which involves levelling the carrier-phase to the code-delay GPS observations and then the IFB estimation; and the so-called arc-by-arc one, which avoids the use of code-delay observations but requires the estimation of arc-dependent biases. Two strategies are used for the analysis: the first one compares calibrated sTEC from two co-located GPS receivers that serve to assess the levelling errors; and the second one, assesses the model error using synthetic data free of calibration error, produced with a specially developed technique. The results show that the arc-by-arc calibration technique performs better than the satellite-by-satellite one for mid-latitudes, while the opposite happens for low-latitudes.

Keywords GPS · Slant total electron content (sTEC) · Inter-frequency biases (IFB) · sTEC calibration

C. Brunini · F. J. Azpilicueta (✉)
Facultad de Ciencias Astronómicas y Geofísicas,
Universidad Nacional de La Plata, Paseo del Bosque,
1900 La Plata, Argentina
e-mail: azpi@fcaglp.unlp.edu.ar

C. Brunini · F. J. Azpilicueta
Consejo Nacional de Investigaciones Científicas y Tecnológicas,
Buenos Aires, Argentina

1 Introduction

The use of the global positioning system (GPS) to study the Earth's ionosphere is continuously expanding. An important credit regarding the popularization of the GPS within the ionospheric community shall be given to the international GNSS service (IGS) (Dow et al. 2005). The availability at the IGS data centres of high quality observations, with almost worldwide coverage and time continuity, has been of great help for many ionospheric studies. Besides, the global ionospheric maps produced by the IGS ionospheric working group (Hernández-Pajares 2004) have become a reference for a variety of ionospheric researches.

The main ionospheric parameter retrieved from the GPS observations is the slant total electron content (sTEC), defined as the integral of the electron density along the satellite to the receiver line of sight (LOS) (Davies and Hartmann 1997). Dual-frequency carrier-phase and code-delay GPS observations can be combined to obtain an ionospheric observable related to the sTEC, s, by the (apparently) simple equation (Ciraolo et al. 2007)

$$L_S = s + b_R + b_S + \mu_A + \varepsilon_L, \tag{1}$$

where the sub-index S refers to a satellite-dependent term, R to a receiver-dependent term, and A to an arc-dependent term, understanding by 'arc' a group of consecutive observations along which the carrier-phase ambiguities do not change. The meaning of the different terms of Eq. 1 will be discussed with more detail in the following paragraphs but, briefly speaking, the definitions are: L_S is the carrier-phase ionospheric observable levelled to the code-delay ionospheric observable; b_R and b_S are the receiver and the satellite inter-frequency biases (IFB) for code-delay observations

(IFB_P);[1] μ_A is the levelling error; and ε_L is the combined effect of the observational noise and the multi-path effects of the raw carrier-phase observations. It is assumed that all the quantities in Eq. 1 are expressed in total electron content units (TECu), 1 TECu is equivalent to 10^{16} electrons per square meter.

The carrier-to-code levelling process is a commonly used procedure to reduce the effects of the carrier-phase ambiguities from the carrier-phase ionospheric observable (Manucci et al. 1999). As it is well known, the code-delay observations are much more affected by the observational noise and the multi-path than the carrier-phase observations, but they are not affected by the ambiguities. Levelling the carrier-phase to the code-delay ionospheric observable consists of shifting every continuous arc of the carrier-phase ionospheric observable by an appropriate constant value (levelling constant) that makes the carrier-phase data match (on average) the noisier but unambiguous code-delay data. Those constant values are interpreted as the effects of the carrier-phase ambiguities on the carrier-phase ionospheric observable. According to Ciraolo et al. (2007), the ambiguities estimated in this way are biased by a systematic arc-dependent error called levelling error (μ_A). The aforementioned paper attributed this error to the superposition of two different effects that are translated to the ambiguities through the levelling process: the presence of multi-path in the code-delay observations and the existence of a temporal variation of the receiver IFB_P that would be correlated with daily changes in the environmental conditions nearby the antenna/receiver. From this, the levelling errors can be mathematically represented as $\mu_A = \langle \varepsilon_P \rangle_A + \langle \delta b_R \rangle_A$, where ε_P is the effect of the multi-path error on the code-delay ionospheric observable; δb_R is the time-varying component of the receiver IFB_P; and the $\langle \cdot \rangle_A$ symbol indicates the average of all the observations within the continuous arc.

According to Eq. 1, the levelled carrier-phase ionospheric observable is affected by biases and errors of different nature. The precision of the measurements is bounded by the observational noise and the multi-path of the raw carrier-phase observations, which are accounted by the term ε_L. This term behaves as an almost random error (not absolutely random because of the presence of the multi-path) with a rather small standard deviation of a few hundredth of TECu. Therefore, the GPS observations are capable of providing very precise sTEC determinations. Nevertheless, the accuracy of the sTEC determinations is not so good, since it depends on the capability of estimating and removing the systematic biases that are present in Eq. 1, i.e., the already mentioned levelling errors (μ_A) and the IFB_P of the receiver (b_R) and the satellites (b_S). These IFB_P are associated to frequency-dependent electronic delays produced in the hardware of the satellites and the receivers. Both together, satellite and receiver IFB_P, may represent a bias of 100 TECu. Therefore, they have to be carefully estimated and removed from the carrier-phase ionospheric observable in order to get an accurate estimation of the sTEC. IFB_P are usually treated as constants for a given period of time (usually 3 days) and estimated from the data themselves, along with the sTEC (Coco et al. 1991; Gaposchkin and Coster 1992; Bishop et al. 1994; Sardon et al. 1994).

In order to assess the magnitude of the levelling errors, Ciraolo et al. (2007) performed an experiment based on the comparison of data gathered from co-located receivers, understanding by 'co-located' a couple of receivers close enough to consider that the sTEC measured from both instruments ought to be the same (see Sect. 3 for details). Under these conditions, making the difference between the levelled carrier-phase ionospheric observables measured to the same arc from both receivers shall produce a quantity free of the sTEC and the satellite-dependent IFB_P. According to Eq. 1, that quantity must primarily (i.e., ignoring the difference between the small ε_L terms) be equal to the sum of two terms: a constant value equal to the difference of the receiver-dependent IFB_P; and an arc-dependent value equal to the difference of the levelling errors of both receivers. Different arcs must display different values according to the levelling errors that affect each arc. In this way, the discrepancies between the different arcs allow assessing the magnitude of the levelling errors. Since these errors are originated by the combination of the code-delay multi-path and the temporal variations of the receiver IFB_P, their magnitudes must depend on the antenna/receiver characteristics. Applying this procedure to different pairs of co-located receivers (different manufacturers and models of GPS receivers and antennas), Ciraolo et al. (2007) estimated levelling errors whose multi-path component ranged from ± 1.4 to ± 5.3 TECu. In the worst case found in that work, the estimation of the time-varying component of the IFB_P reached an amplitude of ± 8.8 TECu (peak-to-peak).

The co-location experiment described by Ciraolo et al. (2007) is good for highlighting the presence of systematic errors in the ionospheric observable, such as the levelling errors pointed out in the preceding paragraph. As a counterpart, the experiment is not good for detecting the presence of errors in the ionospheric model used to estimate the receiver and satellites IFB. As it will be explained in Sect. 3, this type of error is strongly correlated for the two co-located receivers because the LOS are almost coincident. Therefore, making the difference between the calibrated sTEC that is estimated from the levelled observations measured to the same arc from both receivers will cancel the effects of the ionospheric model errors.

[1] The code-delay inter-frequency biases are also known as differential code biases (DCB).

One of the main objectives of this paper is to present a technique capable of assessing the accuracy of the IFB estimation based on the use of synthetic data simulated with an empirical ionospheric model. If these synthetic data, free of levelling errors and IFB, are used as the input of the calibration technique, the differences between the synthetic and the estimated sTEC give the necessary information to assess the accuracy of the technique. The reliability of the technique depends on its ability for creating synthetic data that simulate realistic ionospheric scenarios. Section 4 of this paper will describe the technique for the creation of the ionospheric scenarios that will be used to assess the accuracy of the IFB estimation.

To avoid the undesirable presence of the levelling errors, Ciraolo et al. (2007) suggested the possibility to work with the unlevelled carrier-phase ionospheric observable, L_A (instead of L_S), which implies to change Eq. 1 by

$$L_A = s + b'_R + b'_S + C_A + \varepsilon_L, \tag{2}$$

where b'_R and b'_S are the inter-frequency biases for carrier-phase observations (IFB_L) and C_A is the effect of the carrier-phase ambiguities on the carrier-phase ionospheric observable. The drawback of this approach is the increase of the number of biases and, consequently, the weakness of the estimation reliability as a consequence of the increase of the number of unknowns that have to be estimated from the data: the use of Eq. 1 requires the estimation of one IFB_P per satellite/receiver ($b_R + b_S$), while Eq. 2 requires the estimation of one IFB_L + ambiguity per arc/receiver ($b'_R + b'_S + C_A$). Another important objective of this paper is to assess the accuracy of the calibrated sTEC that is estimated from both, the levelled and the unlevelled carrier-phase ionosphere observables. This issue will be addressed in Sect. 5 of this paper.

2 Biases estimation techniques

The biases estimation technique depends on the procedure chosen to reduce the effect of the carrier-phase ambiguities from the carrier-phase ionospheric observable. The possibility of estimating the ambiguities by performing a geodetic data processing and then reducing their effects from the carrier-phase ionospheric observable (e.g., Hernández-Pajares et al. 2002) will not be considered here. The most commonly used technique relies upon the use of the carrier-to-code levelling procedure, which leads to the levelled carrier-phase ionospheric observable presented in Eq. 1. An alternative technique that will be considered in this section is the one suggested by Ciraolo et al. (2007), i.e., avoiding the levelling process and working with the unlevelled carrier-phase ionospheric observable presented in Eq. 2.

2.1 The thin-layer ionospheric model

The most widely used approach to estimate the IFB—either, the IFB_P from Eq. 1 or the IFB_L and the ambiguity term from Eq. 2—relies upon the so-called thin-layer ionospheric model (e.g., Davies and Hartmann 1997; Manucci et al. 1999). This model approximates the whole ionosphere with a spherical shell of infinitesimal thickness located at an effective given height, h, above the Earth's surface. For this research we adopted a value of 450 km because it has been proved to be good for the South American region (Brunini et al. 2007). The point where the LOS pierces the shell is called the ionospheric penetration point (IPP). The crucial approximation of this approach is the so-called mapping function used to relate the sTEC (s) and the vertical total electron content (vTEC), v, along the vertical line that passes through the IPP. There are different approximations for this mapping function (e.g., Conker and El-Arini 1998) but the simplest one will be considered here

$$\frac{v}{s} = \cos(\theta) = \sqrt{1 - \left(\frac{R}{R+h}\right)^2 \cdot \sin^2(z)}, \tag{3}$$

where R is the mean Earth's radius, z is the LOS zenith angle and θ is the angle between the LOS and the vertical line through the IPP.

The next step in this approach is to choose a suitable mathematical representation of the spatial and temporal variability of the vTEC. Once again, a simple possibility will be used here: a bi-quadratic expansion dependent on the IPP coordinates to represent the spatial variability, and a stepwise function dependent on the Universal Time to represent the temporal variability; mathematically

$$\begin{aligned} v = {} & a_{00}(t) + a_{10}(t) \cdot x + a_{01}(t) \cdot y + a_{20}(t) \cdot x^2 \\ & + a_{11}(t) \cdot x \cdot y + a_{02}(t) \cdot y^2, \end{aligned} \tag{4}$$

where t is the Universal Time and x and y are defined by the relations $x = \lambda_{\mathrm{IPP}} - \lambda_{\mathrm{R}}$ and $y = \mu_{\mathrm{IPP}} - \mu_{\mathrm{R}}$, λ being the geographic longitude and μ being the modip latitude (the sub-indexes IPP refer to IPP location and R to the receiver location). The time-dependent coefficients, $a_{ij}(t)$, are mathematically represented by stepwise functions of the form $a_{ij}(t) = \alpha_{ijk}$, α_{ijk} being a constant for the interval $(t_k, t_k + \Delta t)$ and Δt being the refreshing interval (5 min for this research).

The modip latitude (μ) was firstly proposed by Rawer (1984) for modeling the F2-layer and the top-side ionosphere and it is defined by the relation $\tan(\mu) = I/\sqrt{\cos(\varphi)}$, where I is the magnetic dip at the geographic latitude φ. For a detailed analysis about the benefits of using modip for the representation of the vTEC, the interested reader is referred to Azpilicueta et al. (2005).

Arranging all together, Eqs. 1, 3 and 4 allow obtaining the equation of observation for this problem

$$L_S = \sec(\theta) \cdot \sum_{i=0}^{2} \sum_{j=0}^{2-i} \alpha_{ijk} \cdot x^i \cdot y^j + \beta_S + \varepsilon_L, \quad \text{for} \quad t_k \le t < t_k + \Delta t, \tag{5}$$

where the levelling errors (μ_A) have not been considered, and the receiver and the satellite IFB_P have been combined in a unique satellite-dependent bias, $\beta_S = b_R + b_S$.

Assuming that there are n observations collected along a ΔT interval (3 days for this research). Each one of these observations originates an equation of observation of the form given by Eq. 5 that can be arranged in a linear system of equations of observations

$$\mathbf{A} \cdot \boldsymbol{\alpha} + \mathbf{B}_S \cdot \boldsymbol{\beta}_S = \mathbf{L}_S + \boldsymbol{\varepsilon}_L, \tag{6}$$

where $\boldsymbol{\alpha}$ is a vector of dimension $m_C = 6 \cdot \Delta T / \Delta t$ (5,184 in the case of this research) that contains the α_{ijk} unknowns, and $\boldsymbol{\beta}_S$ is a vector of dimension m_S (the number of observed satellites) that contain the β_S unknowns; $\mathbf{A}$ is the design matrix of dimension $n \times m_C$ for the sTEC expansion (formed by terms of the form $\sec(\theta) \cdot x^i \cdot y^j$ and 0), and $\mathbf{B}_S$ is the design matrix of dimension $n \times m_S$ for the satellite-dependent biases (formed by 1 and 0); finally, $\mathbf{L}_S$ and ε_L are vectors of dimension n that contains the levelled observations (L_S) and their errors (ε_L).

The linear system of Eq. 6 can be solved by the Least Squares method, which originates the following normal system (the supra-index t indicates the transpose matrix operation)

$$\begin{bmatrix} \mathbf{A}^t \cdot \mathbf{A} & \mathbf{A}^t \cdot \mathbf{B}_S \\ \mathbf{B}_S^t \cdot \mathbf{A} & \mathbf{B}_S^t \cdot \mathbf{B}_S \end{bmatrix} \cdot \begin{bmatrix} \hat{\boldsymbol{\alpha}} \\ \hat{\boldsymbol{\beta}}_S \end{bmatrix} = \begin{bmatrix} \mathbf{A}^t \cdot \mathbf{L}_S \\ \mathbf{B}_S^t \cdot \mathbf{L}_S \end{bmatrix}, \tag{7}$$

where $\hat{\boldsymbol{\alpha}}$ and $\hat{\boldsymbol{\beta}}_S$ are the Least Squares estimates of $\boldsymbol{\alpha}$ and $\boldsymbol{\beta}_S$, respectively. In order to focus on the satellite-dependent biases estimation, the normal system of Eq. 7 can be reduced to a completely equivalent system on only the $\boldsymbol{\beta}_S$ unknowns, by applying the Gaussian elimination method on the $\hat{\boldsymbol{\alpha}}$ unknown. This procedure originates the solution

$$\hat{\boldsymbol{\beta}}_S = \mathbf{F}_S \cdot \mathbf{L}_S, \tag{8}$$

where $\mathbf{F}_S = \left(\mathbf{B}_S^t \cdot \mathbf{P} \cdot \mathbf{B}_S\right)^{-1} \cdot \mathbf{B}_S^t \cdot \mathbf{P}$ is the Least Squares pseudo-inverse with a weight matrix equal to $\mathbf{P} = \mathbf{I}_n - \mathbf{A} \cdot \left(\mathbf{A}^t \cdot \mathbf{A}\right)^{-1} \cdot \mathbf{A}^t$ ($\mathbf{I}_n$ is the identity matrix of dimension n). Once the satellite-dependent biases ($\hat{\boldsymbol{\beta}}_S$) are estimated, an estimation of the calibrated sTEC, $\hat{\mathbf{s}}_S$, can be obtained from the levelled observations ($\mathbf{L}_S$)

$$\hat{\mathbf{s}}_S = \mathbf{L}_S - \mathbf{B}_S \cdot \hat{\boldsymbol{\beta}}_S. \tag{9}$$

Applying a similar procedure to Eq. 2 leads to

$$\hat{\boldsymbol{\beta}}_A = \mathbf{F}_A \cdot \mathbf{L}_A, \tag{10}$$

with $\mathbf{F}_A = \left(\mathbf{B}_A^t \cdot \mathbf{P} \cdot \mathbf{B}_A\right)^{-1} \cdot \mathbf{B}_A^t \cdot \mathbf{P}$; and

$$\hat{\mathbf{s}}_A = \mathbf{L}_A - \mathbf{B}_A \cdot \hat{\boldsymbol{\beta}}_A, \tag{11}$$

where the sub-index A indicates the estimation of the arc- instead of the satellite-dependent biases, accordingly to the use of the unlevelled ($\mathbf{L}_A$) instead of the levelled ($\mathbf{L}_S$) observations. The following changes with respect of Eqs. 8 and 9 must be taken into account: $\hat{\boldsymbol{\beta}}_A$ is a vector of dimension m_A (the number of observed arcs) that contains the arc-dependent biases, $\beta_A = b'_R + b'_S + C_A$ (β_A encompasses all together the receiver and the satellite IFB_L and the effect of the carrier-phase ambiguities); and $\mathbf{B}_A$ is the design matrix of dimension $n \times m_A$ for the arc-dependent biases (formed by 1 and 0).

Hereafter, the estimation of the satellite-dependent biases ($\hat{\boldsymbol{\beta}}_S$) from Eq. 8, and the computation of the calibrated sTEC ($\hat{\mathbf{s}}_S$) from Eq. 9, will be called 'the satellite-by-satellite' calibration technique; analogously, the estimation of the arc-dependent biases ($\hat{\boldsymbol{\beta}}_A$) from Eq. 10, and the computation of the calibrated sTEC ($\hat{\mathbf{s}}_A$) from Eq. 11, will be called 'the arc-by-arc' calibration technique.

For the sake of the discussions that will be presented in the next sub-section, it is important to have a closer look at the structure of the design matrices $\mathbf{B}_S$ and $\mathbf{B}_A$ for the satellite- and the arc-dependent biases. As it was already mentioned, these are matrices of dimensions $n \times m_S$ and $n \times m_A$, respectively, formed by 1 and 0. The distribution of 1 and 0 is given by the following conditions: $b_{S,u,v} = 1$ if the observation u corresponds to the satellite v and 0 otherwise; and $b_{A,u,w} = 1$ if the observation u corresponds to the arc w and 0 otherwise.

2.2 The levelling error and the model error effects

For the purpose of assessing the accuracy of the sTEC estimated using the satellite-by-satellite and the arc-by-arc calibration technique, it is convenient to manipulate Eqs. 9 and 11 with the objective of underlining the different kinds of errors that affect one or the other calibration technique. Using the previously defined matrix notation, the Eqs. 1 and 2 can be written as

$$\mathbf{L}_S = \mathbf{s} + \mathbf{B}_S \cdot \boldsymbol{\beta}_S + \mathbf{B}_A \cdot \mu_A + \boldsymbol{\varepsilon}_L, \tag{12}$$

and

$$\mathbf{L}_A = \mathbf{s} + \mathbf{B}_A \cdot \boldsymbol{\beta}_A + \boldsymbol{\varepsilon}_L, \tag{13}$$

where $\mathbf{s}$ is a vector of dimension n that contains the true sTEC. The differences between Eqs. 12 and 13 are the presence of the levelling errors in the first one, and the replacement of the satellite- by the arc-dependent biases in the second one. Replacing $\hat{\boldsymbol{\beta}}_S$ in Eq. 9 by the expression given in Eq. 8; and then replacing $\mathbf{L}_S$ in the resulting formula by the expression given in Eq. 12, the following equation results:

$$\begin{aligned}\hat{\mathbf{s}}_S &= \mathbf{s} + \mathbf{B}_S \cdot \boldsymbol{\beta}_S + \mathbf{B}_A \cdot \boldsymbol{\mu}_A + \boldsymbol{\varepsilon}_L \\ &\quad -\mathbf{B}_S \cdot \mathbf{F}_S \cdot \left(\mathbf{s} + \mathbf{B}_S \cdot \boldsymbol{\beta}_S + \mathbf{B}_A \cdot \boldsymbol{\mu}_A + \boldsymbol{\varepsilon}_L\right) \\ \hat{\mathbf{s}}_S &= \mathbf{s} + \mathbf{B}_S \cdot \boldsymbol{\beta}_S + \mathbf{B}_A \cdot \boldsymbol{\mu}_A + \boldsymbol{\varepsilon}_L \\ &\quad -\mathbf{B}_S \cdot \mathbf{F}_S \cdot \mathbf{s} - \mathbf{B}_S \cdot \mathbf{F}_S \cdot \mathbf{B}_S \cdot \boldsymbol{\beta}_S - \mathbf{B}_S \cdot \mathbf{F}_S \cdot \mathbf{B}_A \cdot \boldsymbol{\mu}_A \\ &\quad -\mathbf{B}_S \cdot \mathbf{F}_S \cdot \boldsymbol{\varepsilon}_L .\end{aligned} \tag{14}$$

In order to interpret the $-\mathbf{B}_S \cdot \mathbf{F}_S \cdot \mathbf{s}$ term of Eq. 14 it is necessary to recall that Eqs. 8 and 9 indicate that the matrix $\mathbf{F}_S$ is a filter (more specifically, the Least Squares filter) that applied on the levelled (but un-calibrated) sTEC observations ($\mathbf{L}_S$) produces the satellite-dependent biases ($\hat{\boldsymbol{\beta}}_S$) that must be used to calibrate the observations and to obtain the calibrated sTEC estimates ($\hat{\mathbf{s}}_S$). If that filter is applied on the true sTEC ($\mathbf{s}$) that is free of errors and calibrations biases, it must produce a satellite-dependent bias equal to 0, i.e., $\mathbf{F}_S \cdot \mathbf{s} = \mathbf{0}$. Any deviation from 0 must be taken as an indication of a mis-functioning of the filter ($\mathbf{F}_S$) that should be attributed to problems in the ionospheric model that is imbedded on it. Therefore, the term $-\mathbf{F}_S \cdot \mathbf{s} = \Delta\hat{\boldsymbol{\beta}}_{S,\mathrm{mod}}$ of Eq. 14 is the error of the estimation of the satellite-dependent biases caused by the ionospheric model errors. Further, this error is translated to the estimation of the calibrated sTEC by means of the term

$$\Delta\hat{\mathbf{s}}_{S,\,\mathrm{mod}} = \mathbf{B}_S \cdot \Delta\hat{\boldsymbol{\beta}}_{S,\,\mathrm{mod}}\,, \quad \text{with } \Delta\hat{\boldsymbol{\beta}}_{S,\,\mathrm{mod}} = -\mathbf{F}_S \cdot \mathbf{s}, \tag{15}$$

in which the $\mathbf{B}_S$ matrix plays the role of a 'distribution operator' that assigns the error $\Delta\hat{\beta}_{S,\mathrm{mod},v}$ of the satellite-dependent bias corresponding to the v satellite to all the calibrated sTEC that is estimated from that satellite.

According to Eq. 14, the levelling errors make two contributions to the estimation of the calibrated sTEC: one is a direct contribution through the term $\mathbf{B}_A \cdot \boldsymbol{\mu}_A$, in which the $\mathbf{B}_A$ matrix plays the role of a 'distribution operator' that assigns the levelling error $\mu_{A,w}$ that affects the w arc to all the calibrated sTEC that is estimated from that arc; and the other is an indirect contribution through the term $\Delta\hat{\boldsymbol{\beta}}_{S,\mathrm{lev}} = -\mathbf{F}_S \cdot \mathbf{B}_A \cdot \boldsymbol{\mu}_A$, which is further translated to the estimation of the calibrated sTEC by means of the term $\mathbf{B}_S \cdot \Delta\hat{\boldsymbol{\beta}}_{S,\mathrm{lev}}$. Both together, these contributions create the term

$$\begin{aligned}\Delta\hat{\mathbf{s}}_{S,\mathrm{lev}} &= \mathbf{B}_A \cdot \boldsymbol{\mu}_A + \mathbf{B}_S \cdot \Delta\hat{\boldsymbol{\beta}}_{S,\mathrm{lev}}, \\ \text{with} \quad \Delta\hat{\boldsymbol{\beta}}_{S,\mathrm{lev}} &= -\mathbf{F}_S \cdot \mathbf{B}_A \cdot \boldsymbol{\mu}_A .\end{aligned} \tag{16}$$

Taking into account the previously given definitions and recalling that $\mathbf{F}_S \cdot \mathbf{B}_S = \mathbf{I}_{m_S}$, Eq. 14 transforms in

$$\hat{\mathbf{s}}_S = \mathbf{s} + \Delta\hat{\mathbf{s}}_{S,\mathrm{mod}} + \Delta\hat{\mathbf{s}}_{S,\mathrm{lev}} + \boldsymbol{\varepsilon}'_L, \tag{17}$$

where $\boldsymbol{\varepsilon}'_L = \boldsymbol{\varepsilon}_L + \boldsymbol{\varepsilon}_{\beta_S}$, with $\boldsymbol{\varepsilon}_{\beta_S} = -\mathbf{B}_S \cdot \mathbf{F}_S \cdot \boldsymbol{\varepsilon}_L$, is the contribution of the observational errors to the errors in the estimation of the calibrated sTEC.

A similar analysis can be performed by substituting Eq. 13 into Eqs. 10 and 11, and then substituting Eq. 10 into 11. In this case, the final result is

$$\hat{\mathbf{s}}_A = \mathbf{s} + \Delta\hat{\mathbf{s}}_{A,\mathrm{mod}} + \varepsilon''_L, \tag{18}$$

where the meaning of the terms

$$\begin{aligned}\Delta\hat{\mathbf{s}}_{A,\mathrm{mod}} &= \mathbf{B}_A \cdot \Delta\hat{\boldsymbol{\beta}}_{A,\mathrm{mod}}, \\ \text{with} \quad \Delta\hat{\boldsymbol{\beta}}_{A,\mathrm{mod}} &= -\mathbf{F}_A \cdot \mathbf{s},\end{aligned} \tag{19}$$

and $\boldsymbol{\varepsilon}''_L = \boldsymbol{\varepsilon}_L + \boldsymbol{\varepsilon}_{\beta_A}$, with $\boldsymbol{\varepsilon}_{\beta_A} = -\mathbf{B}_A \cdot \mathbf{F}_A \cdot \boldsymbol{\varepsilon}_L$, is equivalent to those of Eq. 17, but in this case applied to the arc-by-arc calibration technique. Obviously, the estimation of the calibrated sTEC ($\hat{\mathbf{s}}_A$) from the unlevelled sTEC observations ($\mathbf{L}_A$) is free from the contribution of the levelling error.

With the hope of simplifying the terminology, hereafter the contributions of the ionospheric model errors and the levelling errors to the errors in the estimation of the calibrated sTEC will be, respectively called 'the model error effects' and 'the levelling error effects'.

It is important to distinguish between the model error effects given by Eqs. 15 and 19. Both are a consequence of the errors of the ionospheric model that have been used to calibrate the observations—the thin-layer ionospheric model described in the Sect. 2.1—which are propagated to the calibrated sTEC in a different way by the satellite-by-satellite and the arc-by-arc calibration techniques. Those errors are caused, basically, by two different sources: the mapping function of Eq. 3, used to convert the sTEC into the vTEC at the given IPP; and the mathematical expansion of Eq. 4, used to represent the spatial and the temporal variations of the vTEC. Both error sources are relatively well behaved in the mid-latitude ionospheric region, but their behavior rapidly worsens as soon as the modip latitude gets closer to the low-latitude ionospheric region. These errors are imbedded in the design matrix for the sTEC expansion, $\mathbf{A}$, of Eq. 6 and then, in the weighting matrix, $\mathbf{P}$, and the Least Squares filters, $\mathbf{F}_S$ and $\mathbf{F}_A$, of Eqs. 8 and 10. Therefore, the difference between the model error effects of the satellite-by-satellite and the arc-by-arc calibration techniques arises from the design matrices of the satellite- and the arc-dependent biases, $\mathbf{B}_S$ and $\mathbf{B}_A$, respectively. The first matrix contains, typically, 3 times less columns than the second one ($\mathbf{B}_S$ contains one column for every observed satellite, i.e., $m_S \approx 29$; while $\mathbf{B}_A$ contains one column for every observed arc, i.e., $m_A \approx 100$ for a 3-days observational period). This means that the satellite-by-satellite calibration technique involves the estimation of, roughly, 3 times less calibration bias unknowns than the arc-by-arc calibration technique. It is expected that the increase in the number of unknowns will increase the variance of the unknows.

3 The co-location experiment

In order to assess the magnitude of the levelling error effects, Ciraolo et al. (2007) performed an experiment consisting in the comparison of data from co-located receivers, understanding by 'co-located' a couple of receivers (indicated by the sub-indexes 1 and 2 in Eq. 20) close enough to consider that both instruments are affected by identical sTEC (**s**). According to Eq. 17, the difference of the sTEC estimations, $\hat{\mathbf{s}}_{S,1}$ and $\hat{\mathbf{s}}_{S,2}$, from the two co-located receivers, obtained by means of the satellite-by satellite calibration technique is

$$\hat{\mathbf{s}}_{S,1} - \hat{\mathbf{s}}_{S,2} = \Delta\hat{\mathbf{s}}_{S,\mathrm{mod},1} - \Delta\hat{\mathbf{s}}_{S,\mathrm{mod},2} + \Delta\hat{\mathbf{s}}_{S,\mathrm{lev},1} - \Delta\hat{\mathbf{s}}_{S,\mathrm{lev},2} + \boldsymbol{\varepsilon}'_{L,1} - \boldsymbol{\varepsilon}'_{L,2}, \quad (20)$$

where it was assumed that the observational samples of the receivers 1 and 2 were reduced to the common observations (i.e., $n1 = n2 = n$). The closeness of both receivers (few meters) allows assuming that the matrices $\mathbf{B}_{S,1}$ and $\mathbf{B}_{S,2}$ are identical, as well as the matrices $\mathbf{F}_{S,1}$ and $\mathbf{F}_{S,2}$. Following with this reasoning, the model error effects $\Delta\hat{\mathbf{s}}_{S,\mathrm{mod},1}$ and $\Delta\hat{\mathbf{s}}_{S,\mathrm{mod},2}$ are also identical and Eq. 20 reduces to

$$\hat{\mathbf{s}}_{S,1} - \hat{\mathbf{s}}_{S,2} = \Delta\hat{\mathbf{s}}_{S,\mathrm{lev},1} - \Delta\hat{\mathbf{s}}_{S,\mathrm{lev},2} + \boldsymbol{\varepsilon}'_{L,1} - \boldsymbol{\varepsilon}'_{L,2}. \quad (21)$$

In this equation the levelling error terms dominate over the carrier phase multipath and observational errors. Eq. 21 shows that the co-location experiment is sensitive to the levelling error effects but it is not sensitive to the model error effects. It does not make sense to apply this experiment to the arc-by-arc calibration technique because, according to Eq. 18, the unlevelled observations are free of the levelling error effects.

4 The synthetic dataset

According to the previous section, the co-location experiment cannot provide information about the model error effects on the calibrated sTEC that are estimated by applying either the satellite-by-satellite or the arc-by-arc calibration techniques. This section describes an experiment to accomplish that purpose that relies upon the use of a synthetic sTEC dataset simulated with an empirical ionospheric model, as the input for the Least Squares filters $\mathbf{F}_S$ and $\mathbf{F}_A$ used in the satellite-by-satellite or the arc-by-arc calibration techniques, respectively. By construction, the synthetic dataset is free of the levelling error and the observational noise effects, and is not contaminated by IFB. Therefore, it is possible to assess the model error effects by the simple evaluation of the deviations between the synthetic sTEC data used as input for the Least Squares filter and the calibrated sTEC that are estimated after the filter.

The truthfulness of the assessment obtained through the above mentioned experiment relies upon the ability to create a synthetic dataset that reproduces as realistically as possible the different ionospheric conditions that may happen in the real world. The creation of ionospheric scenarios for model assessment and validation has been scarcely discussed in the literature. This section will follow the guidelines presented by Nava et al. (2005) (further applied by Coïsson et al. 2007), which are based on the use of the NeQuick ionospheric model (Radicella and Leitinger 2001).

The NeQuick model allows computing the electron concentration distribution, $N_e(\varphi, \lambda, h, t, A_Z)$, as a function of the geographic latitude and longitude (φ and λ), the height above the Earth's surface (h), the Universal Time (t) and the effective ionization index, A_Z. The NeQuick package includes specific routines to evaluate the sTEC, $\tilde{s}$, along any LOS, Γ, by a numerical computation of the integral

$$\tilde{s} = \int_{\Gamma} N_e(\varphi, \lambda, h, t, A_Z) \cdot \mathrm{d}\gamma. \quad (22)$$

where $\mathrm{d}\gamma$ is the differential element of the integration path. The NeQuick package has been used by the EGNOS (European Geostationary Navigation Overlay Service) project for assessment analysis and has been adopted for single -frequency operations of the Galileo system. It has also been recommended by the International Telecommunication Union, Radio-communication Sector (ITU-R), as a suitable method for total electron content modeling. The NeQuick code (FORTRAN 77) is available at http://www.itu.int/ITU-R/software/study-groups/rsg3/databanks/ionosph/.

As explained by Nava et al. (2005), the NeQuick model is primarily driven by the effective ionization index (A_Z). Given an A_Z value, the changes of the electron concentration on space and time are controlled by the ITU-R coefficients, which define the shape of the NeQuick vertical profile by determining the values for the peak parameters (the electron concentration and the height of the F2 layer) . Mostly due to this dependence on the ITU-R parameters, the horizontal gradients of the electron concentration computed by the NeQuick model are often smoother than the actual ones. For similar reasons, the time variation of the electron concentration, and consequently the sTEC computed with the NeQuick model, are often smoother than the actual ones.

In order to overcome the previously described limitations of the NeQuick model, Nava et al. (2005) developed a model adaptation technique that relies upon the determination of an effective ionization index, $A_{Z,\mathrm{eff}}$, that minimizes the differences between a set of experimental vTEC values and the corresponding values computed with the NeQuick model. In the aforementioned work, the 'experimental' vTEC values are obtained from GPS observations and are given on a regular grid that span all over the world and the model adaptation

is performed by adjustment of one effective ionization index value per day.

In this research, the model adaptation technique developed by Nava et al. (2005) is modified in order to allow the estimation of an effective ionization index ($A_{Z,\mathrm{eff}}$) for every single observed epoch and from a single GPS receiver. In addition, the minimization of the differences between the modelled and the experimental values is performed in the sTEC domain (instead of in the vTEC domain). A similar approach based also on the NeQuick was proposed and applied by Aragon et al. (2004). As it will be shown in the Sect. 5.2, these modifications contribute to improve the ability of the NeQuick model to reproduce in a more realistic way both, the variation of the sTEC with the LOS zenith angle and the rate of TEC (RoT).

5 Results and discussions

This section is organized in five sub-sections: Sects. 5.1 and 5.2 present the experimental and the synthetic dataset that will be used in the experiments; Sect. 5.3 presents the results of the experiments performed to assess the levelling error effects by using the experimental dataset in connection with the co-location experiment; and Sect. 5.4 presents the experiment performed to assess the model error effects in connection with the synthetic dataset experiment. Finally, Sect. 5.5 considers the combined effects of the levelling and the model errors over the calibrated sTEC estimation.

5.1 The experimental dataset

The experimental dataset encompasses three continuous days of GPS data collected from two co-located receivers in two different locations. The locations are La Plata (57°.93 W, 34°.91 S), Argentina, and Presidente Prudente (51°.41 W, 22°.12 S), Brazil. According to their modip latitude, La Plata site (36°.56 S) is located in the mid-latitude ionospheric region while Presidente Prudente site (26°.28 S) is located in the low-latitude ionospheric region, beneath the southern crest of the Equatorial Anomaly. La Plata site is equipped with two AOA Benchmark ACT GPS receivers with AOA choke-ring antennas and Presidente Prudente site is equipped with two TRIMBLE NetRS GPS receivers with Zephyr Geodetic antennas. The approximate distance between the two antennas is 5 m for the La Plata site and 10 m for the Presidente Prudente one. When necessary, the GPS receivers will be identified with the short names LPGS and LPG2 for the La Plata site and PPTE and LGE1 for Presidente Prudente site. In all the cases, the data sampling rate is 30 s and the cut-off elevation mask is 10°.

The La Plata dataset corresponds to the period from 11 to 13 May 2006 and the Presidente Prudente dataset corresponds to the period from 12 to 14 May 2006. According to the Dst (http://swdcwww.kugi.kyoto-u.ac.jp/dstdir/finalprov.html) and the Kp (http://ftp.gwdg.de/pub/geophys/kp-ap/tab/) geomagnetic indexes, it is a quiet geomagnetic period. From the point of view of the F10.7 solar index (http://www.drao-ofr.hia-iha.nrc-cnrc.gc.ca/icarus/www/solhome.shtml), it corresponds to a low solar activity period.

5.2 The synthetic dataset

The synthetic dataset was created according to the procedure described in Sect. 4. There is a one-to-one correspondence between the experimental and the synthetic data, i.e., every levelled or unlevelled experimental observation computed from the GPS data has a corresponding synthetic observation computed from the NeQuick model. In addition, identical cycle slips have been flagged on both, the experimental and synthetic dataset. This point is important because the number of cycle slips determines the number of unknowns that need to be determined in the arc-by-arc technique and the number of levelling constants for the satellite-by-satellite technique.

The black dot series of Fig. 1 represent the synthetic sTEC, $\tilde{\mathbf{s}}$, computed with the NeQuick model after the adaptation of the effective ionization index, for the La Plata (upper panel) and the Presidente Prudente (lower panel) receivers. The grey dot series represent the difference between the synthetic and the experimental sTEC. The x-axis shows the Local Time for the sites, in hours, from 11 May 2006, 0 h UT. According to the site locations (beneath the Equatorial Anomaly in the case of the Presidente Prudente site and at mid-latitude in the case of the La Plata site), the synthetic–experimental sTEC deviations are greater for the Presidente Prudente than for the La Plata site. As expected, the deviations increase with the LOS zenith angle. Some of the 'tails' that can be observed in Fig. 1 reach values as large as −34 TECu for the La Plata and +43 TECu for the Presidente Prudente site.

Figure 2 shows the RoT for the synthetic sTEC (right-hand side panels) and from the experimental observations (left-hand side panels), for the La Plata (upper panels) and the Presidente Prudente (lower panels) sites. The x-axis shows the Local Time for the sites, in hours, from 11 May 2006, 0 h UT. The comparison of the right- and the left-hand side panels allows a first confirmation that the synthetic data reproduce quite well the main features of the RoT that are present in the experimental data.

The previous results indicate that the synthetic dataset that has been created with the NeQuick model in connection with the model adaptation technique described in Sect. 4, reproduces quite well the outstanding features that are observed in both the sTEC and the RoT that are estimated from the experimental GPS observations. This fact is taken as a satisfactory

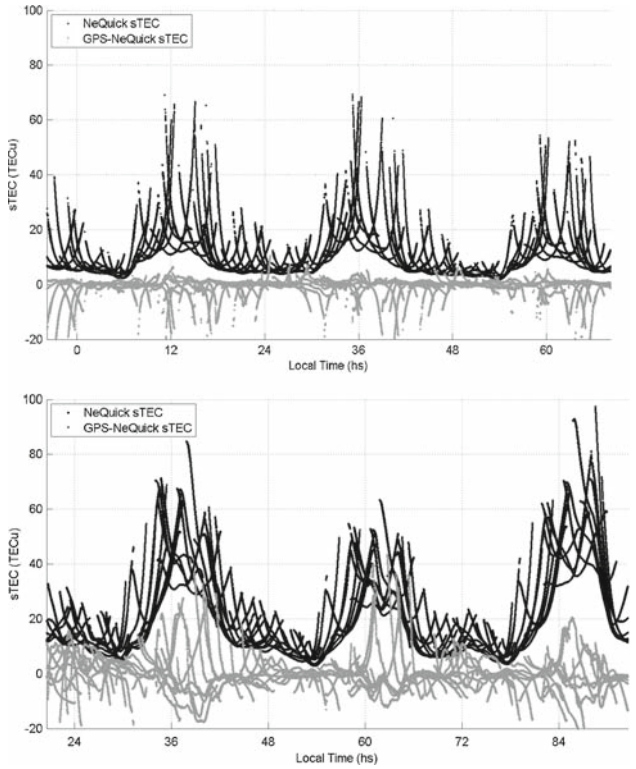

Fig. 1 The synthetic sTEC computed with the NeQuick model after the adaptation of the effective ionization index (*black color*) and the deviations between the synthetic and the experimental sTEC (*grey color*), for the sites of La Plata (*upper panel*) and Presidente] Prudente (*lower panel*)

result from the point of view of the creation of realistic ionospheric scenarios for model assessment and validation studies.

5.3 Assessment of the levelling error effects

The results that will be presented in this sub-section have been obtained from the experimental dataset that was described in Sect. 5.1 and they will be discussed in the theoretical framework that was presented in Sect. 3. The discussion is restricted to the satellite-by-satellite calibration technique, since the arc-by-arc calibration technique is free of the levelling error effects.

Figure 3 shows the differences, $\hat{\mathbf{s}}_{S,1} - \hat{\mathbf{s}}_{S,2}$, of the calibrated sTEC estimations obtained with the satellite-by-satellite calibration technique using observations from the two co-located receivers placed at the La Plata (LPGS–LPG2, upper panel) and the Presidente Prudente (PPTE–LGE1, bottom panel) sites. The grey scale corresponds to the different satellites (29 in this case) that were present in the dataset. The x-axis shows the Local Time for the sites, in hours, from 11 May 2006, 0 h UT. According to Eq. 21, the difference $\hat{\mathbf{s}}_{S,1} - \hat{\mathbf{s}}_{S,2}$ is dominated by the combination of the levelling error effects, $\Delta\hat{\mathbf{s}}_{S,\mathrm{lev},1}$ and $\Delta\hat{\mathbf{s}}_{S,\mathrm{lev},2}$, in both receivers. The time-varying component of the levelling errors can be recognized in the La Plata plot as a decreasing linear trend (upper panel). This effect is not apparent in the Presidente Prudente plot (bottom panel). The effect of the multi-path components of the levelling errors, $\langle \varepsilon_{P,1} \rangle_A$ and $\langle \varepsilon_{P,2} \rangle_A$, can be clearly noted as a combination of a periodic daily variation for the La Plata plot and in both figures as a spread between the different groups of data that correspond to the different satellites arcs. The plots also show a noise of small amplitude that come out from the observational errors of the carrier-phase measurements.

Under the assumption that the standard deviation for the levelling error on both co-located receivers is the same, i.e., $\mathrm{StdDev}(\Delta\hat{\mathbf{s}}_{S,\mathrm{lev},1}) = \mathrm{StdDev}(\Delta\hat{\mathbf{s}}_{S,\mathrm{lev},2}) \equiv \mathrm{StdDev}(\Delta\hat{\mathbf{s}}_{S,\mathrm{lev},2})$; Eq. 21 leads to $\mathrm{StdDev}(\hat{\mathbf{s}}_{S,1} - \hat{\mathbf{s}}_{S,2}) = \mathrm{StdDev}(\Delta\hat{\mathbf{s}}_{S,\mathrm{lev},1} - \Delta\hat{\mathbf{s}}_{S,\mathrm{lev},2}) = \sqrt{2} \cdot \mathrm{StdDev}(\Delta\hat{\mathbf{s}}_{S,\mathrm{lev}})$; and then $\mathrm{StdDev}(\Delta\hat{\mathbf{s}}_{S,\mathrm{lev}}) = \frac{\mathrm{StdDev}(\hat{\mathbf{s}}_{S,1} - \hat{\mathbf{s}}_{S,2})}{\sqrt{2}}$. Figure 4 shows the cumulative distribution of the levelling error effects, in absolute value, for a single receiver, computed from the previously stated equation. The results for the La Plata (LPGS) site are shown with a dashed line and the corresponding results for the Presidente Prudente (PPTE) site are shown with a solid line. According to these distributions, 95% of the samples are below ± 1.6 TECu for the La Plata site and below ± 0.5 TECu for the Presidente Prudente site. These values depend on the receiver–antenna configurations that are installed on each site and on the environmental conditions that surround the antennas and may cause multi-path effects and/or fluctuations of the IFB_P. In any case, these values should be taken as indicators of the level of accuracy that can achieve the sTEC estimated from the levelled ionospheric observable by using the satellite-by-satellite calibration technique in connection with the thin-layer ionospheric model described in Sect. 2.1 of this paper.

5.4 Assessment of the model error effects

As it was explained in Sect. 3, the co-location experiment is good for highlighting the levelling error effects but it is not sensitive to the model error effects. This sub-section is devoted to assess the model error effects by applying the synthetic dataset experiment described in Sect. 4 and using the synthetic dataset described in Sect. 5.2. The assessment will be performed for both, the calibrated sTEC estimated by means of the satellite-by-satellite and the arc-by-arc calibration techniques.

After the development presented in Sect. 2.2, the model error effects can be expressed by $\Delta\hat{\mathbf{s}}_{S,\mathrm{mod}} = -\mathbf{B}_S \cdot \mathbf{F}_S \cdot \tilde{\mathbf{s}}$ for the satellite-by-satellite technique, and by $\Delta\hat{\mathbf{s}}_{A,\mathrm{mod}} = -\mathbf{B}_A \cdot \mathbf{F}_A \cdot \tilde{\mathbf{s}}$, for the arc-by-arc technique, where $\tilde{\mathbf{s}}$ represents the synthetic sTEC observations. Figure 5 shows the model error effects for the satellite-by-satellite (right-hand

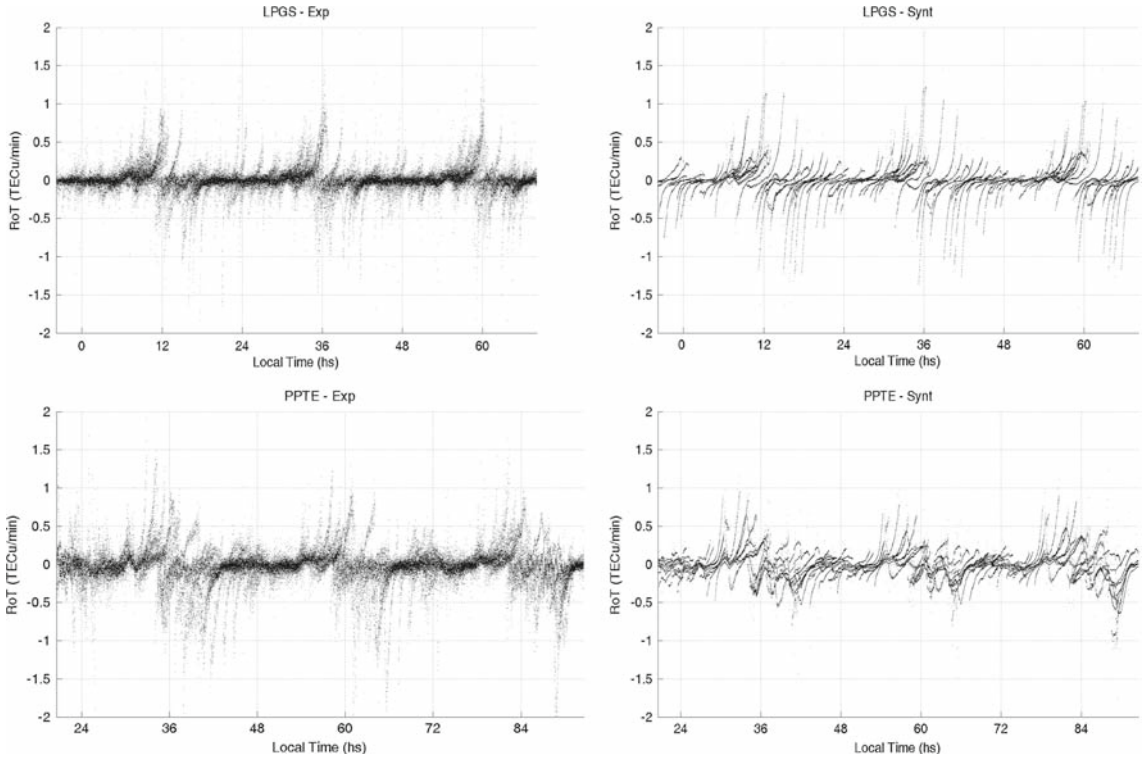

Fig. 2 The rate of change of the sTEC (RoT) for the experimental data (*right-hand side panels*) and for the synthetic data (*left-hand side panels*) for the sites of La Plata (*upper panels*) and Presidente Prudente (*lower panels*)

side panels) and the arc-by-arc (left-hand side panels) calibration techniques, for the site of La Plata (upper panels) and Presidente Prudente (lower panels) sites. The grey scale corresponds to the different satellites (29 in this case) that were present in the dataset. The x-axis shows the Local Time for the sites, in hours, from 11 May 2006, 0 h UT. From the inspection of Fig. 5 it is apparent that the model error effects are greater for the site of Presidente Prudente (lower panels) than for the site of La Plata (upper panels). This is in accordance with the higher complexity of the physical processes that control the sTEC variability in the low-latitude ionosphere region in respect of the mid-latitude one. As discussed in Sect. 2.2, both the mapping function used to convert the sTEC into the vTEC and the mathematical expansion used to represent the spatial and the temporal variations of the vTEC, perform better at mid- than at low-latitude.

Figure 6 shows the histogram of the model error effects for the site of La Plata (upper panel) and Presidente Prudente (lower panel), for the satellite-by-satellite (solid lines) and the arc-by-arc (dashed lines) calibration techniques. The main conclusions that can be extracted from these distributions are:

(i) For a mid-latitude site (La Plata), both calibration techniques are similarly affected by the model errors, being the arc-by-arc slightly less affected than the satellite-by-satellite one; 95% of the model error effects are confined between approximately −2.5 and +2.5 TECu in the first case, and between approximately −3.0 and +2.0 in the second case (the average values of the model error effects are −0.2 and +0.4 TECu, respectively).

(ii) For a low-latitude site (Presidente Prudente), the satellite-by-satellite is less affected by the model errors than the arc-by-arc calibration technique; 95% of the model error effects are confined between approximately −5.0 and +4.5 TECu in the first case, and between approximately −5.5 and +7.5 TECu in the second case (the average values of the model error effects are +0.5 and +0.3 TECu, respectively).

5.5 Assessment of the combined levelling and model error effects

When the satellite-by-satellite calibration technique is applied to the experimental data, the levelling and model error effects act simultaneously. From the results obtained in the previous two sections as summarized in Table 1, the satellite-by-satellite calibration technique will produce calibrated sTEC estimation with an uncertainty (95% of confidence) between approximately −4.6 and +3.6 for the La Plata site, and between approximately −5.5 and +5.0 TECu for the

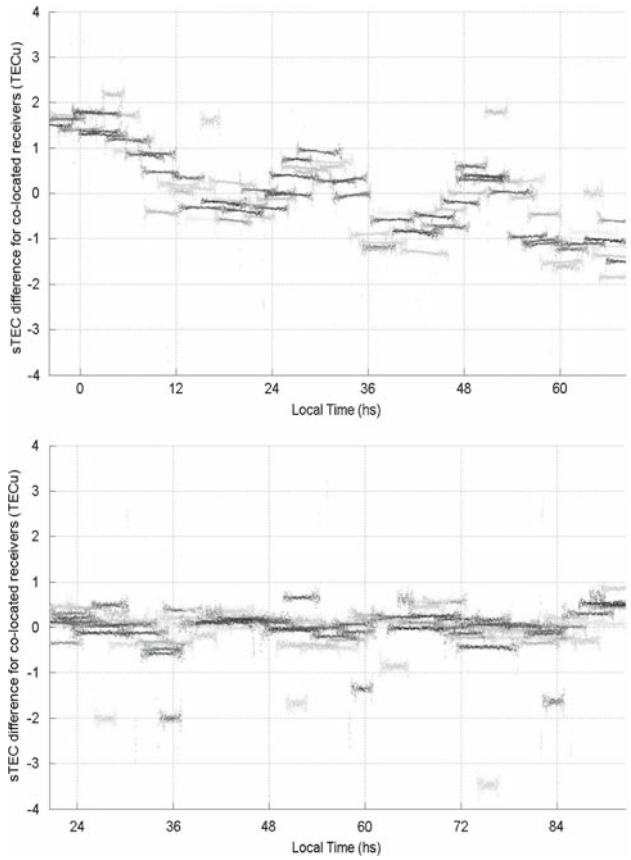

Fig. 3 The differences of the calibrated sTEC estimation obtained with the satellite-by-satellite calibration technique using observations from the two co-located receivers placed at the sites of La Plata (LPGS–LPG2, *upper panel*) and Presidente Prudente (PPTE–LGE1, *bottom panel*). The *grey scale* corresponds to the different satellites (29 in this case) that were present in the dataset

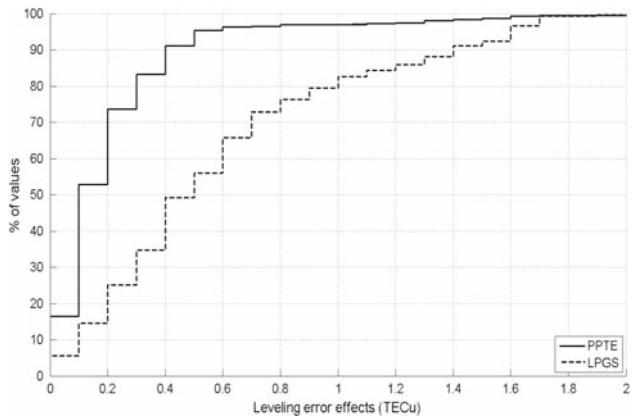

Fig. 4 The cumulative distribution of the levelling error effects, in absolute value, for a single receiver in the sites of La Plata (LPGS, *dashed line*) and Presidente Prudente (PPTE, *solid line*)

Presidente Prudente site. These values are obtained as the worst combination of the levelling and model errors. When the arc-by-arc calibration technique is applied to experimental data, the levelling error effects do not apply and only the model error effects shall be considered. Thus, the calibrated sTEC that are estimated with this technique are affected by an uncertainty (95% of confidence) between approximately −2.5 and +2.5 TECu for the La Plata site, and between approximately −5.5 and +7.5 TECu for the Presidente Prudente site. The third column of Table 1 resumes the results obtained in this sub-section.

6 Summary and conclusions

The GPS observations can provide very precise sTEC determinations but the accuracy of those determinations depends on the reliability of the calibration biases that must be determined and reduced from the observations in order to get calibrated sTEC values. Those calibration biases have to be estimated from the observations themselves and it requires the use of an ionospheric model, whose errors are unavoidably propagated to the estimated calibration biases and, consequently, to the calibrated sTEC estimation.

The main objective of this research was to compare the so-called satellite-by-satellite and arc-by-arc calibration techniques. The benefit of the second one in respect of the first technique is the use of the unlevelled observations that are free from the leveling error effects, as suggested by Ciraolo et al. (2007). Its drawback is the need of estimating a major number of unknowns: while the use of the levelled observations requires the estimation of one calibration bias (which encompasses the satellite and receiver IFB_P) for every observed satellite (hence the appellation 'satellite-by-satellite'), the use of the unlevelled observations demands the estimation of one calibration bias (which encompasses the satellite and the receiver IFB_L and the carrier-phase ambiguity) for every observed arc (hence the appellation 'arc-by-arc'). It is expected that the increase of the number of unknowns that have to be estimated from the same amount of data would cause worse propagation of the model formal errors to the unknowns.

Ciraolo et al. (2007) performed an experiment based on the comparison of the sTEC estimated from two nearby receivers. In absence of the levelling errors, the difference between the sTEC estimated from both receivers to a given satellite must be equal to the difference between the IFB_P of those receivers. This so-called co-location experiment is a good approach to assess the levelling error effects but, as it was demonstrated in this research, it is not sensitive to the model error effects. In order to get a reliable estimation of the model error effects, it was necessary to develop a suitable technique for creating realistic ionospheric scenarios. That technique relied upon the use of the NeQuick ionospheric model and was based on a previous work by Nava et al. (2005) and Aragon et al. (2004).

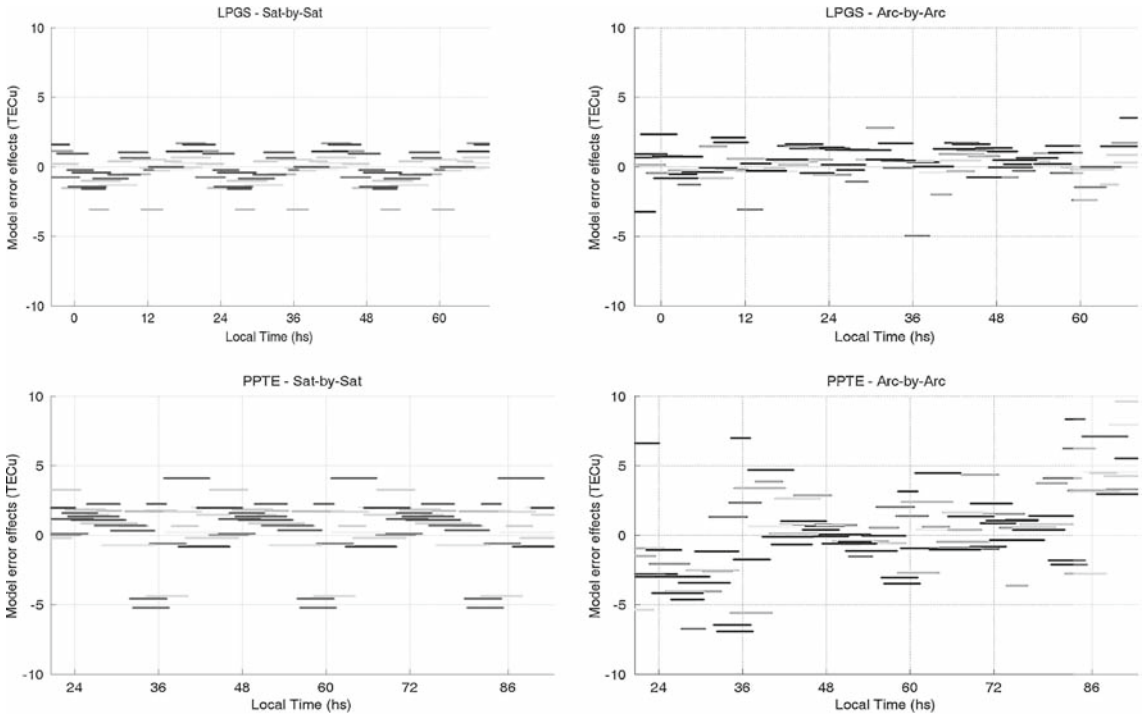

Fig. 5 The model error effects for the satellite-by-satellite (*right-hand side panels*) and for the arc-by-arc (*left-hand side panels*) calibration techniques, for the sites of La Plata (*upper panels*) and Presidente Prudente (*lower panels*). The *grey scale* corresponds to the different satellites (29 in this case) that were present in the dataset

The experiments presented in this paper were based on experimental and synthetic datasets corresponding to two co-located GPS receivers in two different places: one in the mid-latitude region (La Plata, Argentina) and the other in the low-latitude region, beneath the southern crest of the Equatorial Anomaly (Presidente Prudente, Brazil). The dataset encompassed three continuous days in May 2006 that correspond to a low solar activity and quiet geomagnetic conditions period. The truthfulness of the synthetic dataset created with the developed model adaptation technique was evaluated by comparing the synthetic sTEC and RoT to the corresponding values obtained from experimental (GPS-based) data. The agreement between synthetic and experimental values was better for the mid-latitude than for the low-latitude region, but even in the second case the results were judged as satisfactory.

The levelling error effects were evaluated from the experimental GPS data gathered from two co-located receivers. According to this experiment, the levelling errors are ± 1.6 TECu for the La Plata site and ± 0.5 TECu for the Presidente Prudente site (95% of the samples). These values depend on the receiver–antenna configurations that are installed on each site and on the environmental conditions that surround the antennas and may cause multi-path effects and/or fluctuations of the IFB_P. They must be taken as indicators of the accuracy level of the sTEC estimated from the levelled ionospheric observable by using the satellite-by-satellite calibration technique in connection with the thin-layer ionospheric model.

The model error effects were evaluated from the synthetic data created with the adapted NeQuick model. As expected, they are greater for the low-latitude than for the mid-latitude site. This fact is attributed to the limitations of the mapping function and the mathematical expansion used to represent the vTEC to cope with the complex equatorial anomaly behaviors. The satellite-by-satellite and the arc-by-arc calibration techniques perform quite well for the mid-latitude region, where the model error effects are confined to -3.0 and $+2.0$ TECu in the first case, and to -2.5 and $+2.5$ TECu in the second case (95% of the samples). In the low-latitude region the satellite-by-satellite calibration technique performs better than the arc-by-arc one. The model error effects are confined to -5.0 and $+4.5$ TECu in the first case and to -5.5 and $+7.5$ TECu in the second case. The fact that both calibrations techniques produce similar results in the mid-latitude region is attributed to the relatively good performance of the thin-layer ionospheric model in that region. The performance of the model deteriorates in the low-latitude region and the

Table 1 Summary of the accuracy assessment (95% of confidence) for the model error, the levelling error and the combined effect on the satellite-by-satellite and the arc-by-arc calibration techniques, for both analyzed regions

	Model error (TECu)	Levelling error (TECu)	Combined error (TECu)
Satellite-by-satellite			
Mid-latitude	−3.0 to +2.0	± 1.6	−4.6 to 3.6
Low-latitude	−5.0 to +4.5	± 0.5	−5.5 to 5.0
Arc-by-arc			
Mid-latitude	−2.5 to +2.5	–	−2.5 to +2.5
Low-latitude	−5.5 to +7.5	–	−5.5 to +7.5

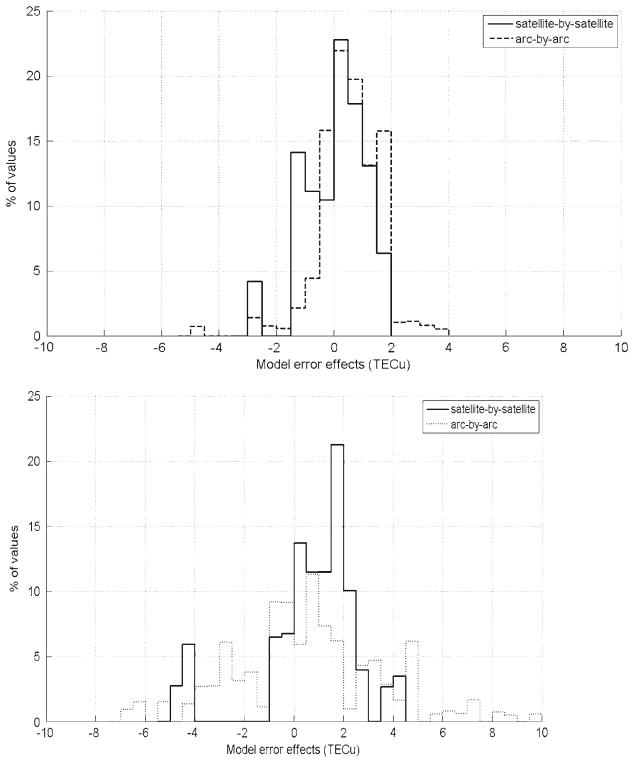

Fig. 6 The distribution of the model error effects for the sites of La Plata (*upper panel*) and Presidente Prudente (*lower panel*), for the satellite-by-satellite (*solid lines*) and the arc-by-arc (*dashed lines*) calibration techniques

larger errors that occur there are worse propagated by the arc-by-arc than by the satellite-by-satellite calibration technique.

When the satellite-by-satellite calibration technique is applied to real data, both model and levelling errors act simultaneously and their effects must be added. This is not the case for the arc-by-arc calibration technique, which is affected by the model but not by the levelling errors. These considerations lead to the assessment of the sTEC estimation accuracy (95% of confidence) given in the third column of Table 1. It can be concluded that the arc-by-arc calibration technique performs better than the satellite-by-satellite one for mid-latitudes (reduction of ∼40% of the uncertainty) while the opposite happens for low-latitudes (increase of ∼23% of the uncertainty). The balance between the levelling and the model error effects may change for different GPS instruments (receivers and antennas), different environmental conditions (multi-path) and different ionospheric conditions (season, solar activity, geomagnetic disturbances). The results presented here must be taken as a first assessment of their impact on the accuracy of the GPS-based sTEC estimations. Besides, the technique to create the synthetic dataset presented in this work could be a valuable tool for error assessment and model validation. A research is currently undergoing to upgrade that technique in order to account for ionospheric storm effects.

Acknowledgments The authors wish to thank Professors João Francisco Galera Mônico and Paulo de Oliveira Camargo, from the Universidad Estadual Paulista (Brazil), for kindly providing the GPS data of the Presidente Prudente stations and for the constructive discussions sustained in the framework of the joint project 'Uma contribuição para o desenvolvimento científico e acadêmico na América do Sul para o uso eficiente do Sistema de Navegação Global por Satélites (GNSS)'. The support of the joint cooperation program between the SECyT (Argentina) and the CAPES (Brazil) is also acknowledged. The authors would like to thank Dr. Henandez-Pajares for improving the quality of our manuscript with his comments and suggestions and Dr. Klees and Dr. Boehm, Editor-in-chief and Editor of the Journal, for their recommendations.

References

Aragón A, Orús R, Amarillo F, Hernández-Pajares M, Juan JM, Sanz J (2004) Performance of NeQuick ionospheric predictions compared with different ionospheric data. Presented at ESTEC/ESA Navitech'04, Noordwijk

Azpilicueta F, Brunini C, Radicella S (2005) Global ionospheric maps from GPS observations using modip latitude. JASR. doi:10.1016/j.asr.2005.07.069

Bishop G, Walsh D, Daly P, Mazzella A, Holland E (1994) Analysis of the temporal stability of GPS and GLONASS group delay correction terms seen in various sets of ionospheric delay data. In: Proceeding of the ION GPS-94, pp 1653–1661

Brown RG, Hwang PYC (1992) Introduction to random signals and applied Kalman filtering, 2nd edn. Wiley, London

Brunini C, Meza A, Gende M, Azpilicueta F (2007) South American regional ionospheric maps computed by GESA: a pilot service in the framework of SIRGAS. JASR 42:737–744. doi:10.1016/j.asr.2007.08.041

Ciraolo L, Azpilicueta F, Brunini C, Meza A, Radicela SM (2007) Calibration errors on experimental slant total electron content determined with GPS. J Geod 81(2):111–120. doi:10.1007/s00190-006-0093-1

Coco DS, Coker C, Dahlke SR, Clynch JR (1991) Variability of GPS satellite differential group delays biases. IEEE Trans Aerosp Electron Syst 27(6):931–938. doi:10.1109/7.104264

Coïsson P, Radicella SM, Nava B (2007) Use of the NeQuick model for ionospheric scenarios generation. Presented at the IUGG general assembly, Perugia

Conker R, El-Arini MB (1998) A novel approach for an ionospheric obliquity process responsive to azimuthal variation. Presented at the ION-GPS-98, Nashville

Davies K, Hartmann GK (1997) Studying the ionosphere with the global positioning system. Radio Sci 32(4):1695–1703. doi:10.1029/97RS00451

Dow JM, Neilan RE, Gendt G (2005) The international GPS service (IGS): celebrating the 10th anniversary and looking to the next decade. JASR 36(3):320–326. doi:10.1016/j.asr.2005.05.125

Goposchkin EM, Coster AJ (1992) GPS L1-L2 bias determination. In: Proceeding international beacon satellite symposium, Massachusetts

Hernandez-Pajares M (2004) IGS ionosphere WG: an overview. In: Proceeding COST 2004, Nice, pp 29–29

Hernández-Pajares M, Juan JM, Sanz J, Colombo O (2002) Improvig the real-time ionopsheric determination from GPS sites at very long distances over the equator. J Geophys Res. doi:10.1029/2001JA009203

Manucci AJ, Iijima BA, Lindqwister UJ, Pi X, Sparks L, Wilson BD (1999) GPS and ionosphere. URSI reviews of radio science, Jet Propulsion Laboratory, Pasadena

Nava B, Coïsson P, Miró Amarante G, Azpilicueta F, Radicella SM (2005) A model assisted ionospheric electron density reconstruction method based on vertical TEC data ingestion. Ann Geophys 48(2):313–320

Radicella SM, Leitinger R (2001) The evolution of the DGR approach to model electron density profiles. JASR 27(1):35–40. doi:10.1016/S0273-1177(00)00138-1

Rawer K (ed) (1984) Encyclopedia of physics. Geophysics III, Part VII. Springer, Heidelberg, pp 389–391

Sardon E, Rius A, Zarraoa N (1994) Estimation of the transmitter and receiver differential biases and the ionospheric total electron content from global positioning system observations. Radio Sci 29:577–586. doi:10.1029/94RS00449